Theoretical analysis of a quartz-enhanced photoacoustic spectroscopy sensor

N. Petra · J. Zweck · A.A. Kosterev · S.E. Minkoff · D. Thomazy

Abstract Quartz-enhanced photoacoustic spectroscopy (QEPAS) sensors are based on a recent approach to photoacoustic detection which employs a quartz tuning fork as an acoustic transducer. These sensors enable detection of trace gases for air quality monitoring, industrial process control, and medical diagnostics. To detect a trace gas, modulated laser radiation is directed between the tines of a tuning fork. The optical energy absorbed by the gas results in a periodic thermal expansion which gives rise to a weak acoustic pressure wave. This pressure wave excites a resonant vibration of the tuning fork thereby generating an electrical signal via the piezoelectric effect. This paper describes a theoretical model of a QEPAS sensor. By deriving analytical solutions for the partial differential equations in the model, we obtain a formula for the piezoelectric current in terms of the optical, mechanical, and electrical parameters of the system. We use the model to calculate the optimal position of the laser beam with respect to the tuning fork and the phase of the piezoelectric current. We also show that a QEPAS transducer with a particular 32.8 kHz tuning fork is 2–3 times as sensitive as one with a 4.25 kHz tuning fork. These simulation results closely match experimental data.

PACS 42.62.Fi · 43.38.Zp · 43.38.Fx

N. Petra (✉) · J. Zweck · S.E. Minkoff
Department of Mathematics and Statistics, University of
Maryland, Baltimore County, 1000 Hilltop Circle, Baltimore,
MD 21250, USA
e-mail: znoemi1@umbc.edu
Fax: +1-410-4551066

A.A. Kosterev · D. Thomazy
Department of Electrical and Computer Engineering, Rice
University, 6100 Main Street, Houston, TX 77251, USA

1 Introduction

Sensor systems that detect and quantify the concentration of specific trace gases will become essential components of urban air quality monitoring, industrial process control, and medical diagnostics using breath biomarkers [1–3]. Recently, there has been a growing interest in quartz-enhanced photoacoustic spectroscopy (QEPAS) sensors which use a quartz tuning fork (QTF) as a resonant acoustic transducer [4]. A QEPAS sensor detects the weak acoustic pressure wave that is generated when optical radiation is absorbed by a trace gas. This pressure wave excites a resonant vibration of a quartz tuning fork, which is then converted into an electrical signal (charge separation on the electrodes of the tuning fork) due to the piezoelectric effect. Then, a transimpedance amplifier is usually used to make a virtual short circuit between the electrodes and to measure the generated current, which is proportional to the concentration of the gas. Experimental studies show high sensitivity of QEPAS which, combined with a miniature sensor size and immunity to environmental acoustic noise, makes this technology an attractive alternative to other trace gas sensing methods [1, 5, 6].

The majority of reported QEPAS-based sensor configurations include a spectrophone (the module for detecting laser-induced sound) consisting of a QTF and a microresonator composed of a pair of thin tubes [4, 5]. Experiments have shown that the microresonator yields a signal gain of 10 to 20. However, there are some situations in which it is advantageous to use the simplest spectrophone configuration consisting of the QTF alone. These situations include the use of optical sources with low spatial radiation quality (multimode lasers, LEDs), or when extremely local sensing is needed. The theoretical analysis developed in this paper concerns this simplest QEPAS spectrophone. The theory

will enable future comparisons between QEPAS transducers based on various commercially available QTFs without performing actual gas-sensing experiments.

The theoretical analysis of QEPAS sensors relies on the theory of photoacoustic spectroscopy [7–9] and the mechanical and piezoelectric properties of quartz tuning forks [10–12]. Miklos et al. [9] described experimental and theoretical investigations of photoacoustic signal generation in which a gas-filled resonant acoustic cavity (rather than a quartz tuning fork) is used to accumulate the energy from a photoacoustic signal. Karraï and Grober [10] discussed a theoretical model for the application of tuning fork sensors to atomic-force and optical near-field microscopy. In these applications the vibration of the tuning fork is induced by a point force concentrated at the tip of the tuning fork, whereas in a QEPAS sensor the pressure-induced driving force is distributed over the inner and outer surfaces of each tine. Until now, the only theoretical model of a QEPAS sensor is that of Wojcik et al. [13] who studied a trace-gas sensor that combines an amplitude-modulated quantum cascade laser with a QEPAS sensor. However, they did not use their model to quantify how the amplitude or phase of the received electrical signal depends on the system parameters.

In this paper we describe a theoretical model for a wavelength-modulated QEPAS sensor currently being developed by Kosterev et al. [1, 4, 5]. Our QEPAS model consists of three stages. First, we model the propagation of the acoustic wave in space. We calculate an explicit formula for the acoustic pressure wave by using the cylindrical symmetry of the laser beam and the narrow width of the tuning fork resonance to reduce the inhomogeneous wave equation to a Bessel equation. This approach is much simpler than that of Wojcik et al. [13] who relied on the three-dimensional Green's function solution of the wave equation. The solution we derive shows that the amplitude of the pressure wave is proportional to the laser modulation frequency. Second, we use the Euler–Bernoulli equation forced by the acoustic pressure to model the resonant vibration of the tines of the tuning fork. Finally, we use well-known electromechanical relationships for quartz tuning forks to calculate the piezoelectric current generated by this mechanical vibration [12]. We note that Wojcik et al. [13] gave a brief description of the second and third stages of the model.

To validate the model and study the dependence of the piezoelectric signal strength on the system parameters we use the theory and experiments to determine the amplitude and phase of the piezoelectric current as functions of the position of the laser beam. Our model shows that the theoretical calculation and experimental measurements of a normalized amplitude function and of the phase are in very good agreement. However, in absolute units the theoretically calculated signal strength is about two times smaller than that

measured in experiments. One possible reason for this discrepancy is that we did not include the effect that the tuning fork has on the pressure-wave solution.

We also investigate how the sensitivity of the QEPAS transducer is affected by the resonance frequency of the tuning fork by comparing results from particular 32.8 kHz and 4.25 kHz tuning forks. Our theoretical and experimental results show that the piezoelectric signal strength obtained using the 32.8 kHz tuning fork is 2–3 times as large as that obtained from the 4.25 kHz tuning fork.

In Sect. 2, we describe our theoretical model for a QEPAS sensor and derive analytical solutions of the partial differential equations involved in the model. In Sect. 3, we validate the model by comparison to experiments and study the dependence of the signal strength on the system parameters. Finally, in Sect. 4 we summarize our results and briefly discuss future extensions of the model.

2 Mathematical model

Several experimental configurations for QEPAS sensors are discussed in [4]. In this paper we study the configuration in which the laser beam is focused between the tines of the tuning fork and there is no gas-filled acoustic microresonator cavity. We now explain the three stages of a simple model of a QEPAS sensor.

2.1 Model of the optically generated acoustic wave

We model the acoustic pressure wave generated by the interaction of the laser beam with the trace gas by regarding it as a wave that propagates in all of space, and in particular assume that it is not influenced by the tuning fork. As a first approximation this assumption is reasonable since the wavelength of the pressure wave is approximately 10^{-2} m, which is large compared to the thickness and width of the tuning fork that are both less than 10^{-3} m. The acoustic pressure, P, in space satisfies the acoustic wave equation

$$\frac{\partial^2 P}{\partial t^2} - c^2 \Delta P = S, \tag{1}$$

where t is time and c is the sound speed. The acoustic source term, S, is given by $S = (\gamma - 1)(\partial H/\partial t)$, where γ is the adiabatic coefficient of the gas and $H = \kappa I$ is the heat power density deposited in the gas [14]. Here κ is the absorption per unit length along the laser beam and I is the laser power density per unit cross-sectional area of the beam. We assume that the laser beam is a Gaussian beam of constant width, σ. This assumption is reasonable since the Rayleigh range of the beam is about 20 mm whereas the thickness of the tuning fork is less than 1 mm, and so the width of the

beam is approximately constant in the vicinity of the tuning fork. Therefore, the laser power density is of the form $I(r) = W_L g(r)$, where $g(r) = \exp(-r^2/2\sigma^2)/2\pi\sigma^2$ is the normalized power density and W_L is the laser power. Here r is the radial distance from the axis of the beam.

QEPAS systems use either wavelength- or amplitude-modulated lasers. In this work, we modulate the wavelength of the laser back and forth across the absorption line of the gas to be detected, which we model as $\lambda(t) = \lambda_c + \lambda_{amp} \sin(2\pi f t/2)$, where λ_{amp} is the amplitude of oscillation about the central wavelength λ_c. The frequency of this oscillation is chosen to be half the resonant frequency, f, of the tuning fork. If we let $\widetilde{\kappa}(\lambda)$ denote the absorption spectrum of the gas, then the absorption of laser radiation is described by $\kappa(t) = \widetilde{\kappa}(\lambda(t))$. A QTF is a sharply resonant receiver and can detect only signals whose frequency is at or very close to the resonance frequency, f. Therefore, we consider only the second Fourier component, κ_f, of κ, which can be expressed as

$$\kappa_f(t) = \frac{\kappa_{eff}}{2} \cos(2\pi f t - \phi),$$

where

$$\kappa_{eff} = \frac{2}{T} \left| \int_{-T}^{T} \kappa(t) \exp(2\pi i f t) \, dt \right|$$
$$= \frac{2}{\pi} \left| \int_{-\pi}^{\pi} \widetilde{\kappa}(\lambda_c + \lambda_{amp} \sin s) \exp(2is) \, ds \right|, \quad (2)$$

where $T = 1/f$. Equation (2) shows that κ_{eff} does not depend on the modulation frequency, f. We assume that $\phi = 0$, since in the experiments $\widetilde{\kappa}(\lambda)$ is symmetric about $\lambda = \lambda_c$ when $\lambda_c - \lambda_{amp} \leq \lambda \leq \lambda_c + \lambda_{amp}$, and so $\kappa_f(t)$ is even. We choose the source function S in (1) to be

$$S = W \exp(-r^2/2\sigma^2) \exp(i\omega t), \quad (3)$$

where $\omega = 2\pi f$ and

$$W = -(\gamma - 1) \frac{\kappa_{eff}}{2} \frac{W_L}{2\pi\sigma^2} \omega, \quad (4)$$

so that the pressure wave is given by the imaginary part of the solution of (1).

In the case of amplitude modulation, (4) is replaced by $W = -(\gamma - 1)(\widetilde{\kappa}(\lambda_c)/2)(W_{max}/2\pi\sigma^2)\omega$, where W_{max} is the maximum laser power. If $\widetilde{\kappa}$ is a Lorentzian with a full-width at half-maximum of λ_{FWHM}, the maximum value of κ_{eff} is 70% of $\widetilde{\kappa}(\lambda_c)$ and occurs when $\lambda_{amp} = 1.1\lambda_{FWHM}$.

Because the frequency width of the resonance of the tuning fork is extremely narrow (the Q-factor exceeds 10 000) and because of the cylindrical symmetry of the Gaussian beam it is sufficient to work with a steady-state solution of (1) of the form $P(r,t) = p(r)\exp(i\omega t)$. Substituting P

into (1) we obtain the inhomogeneous Bessel equation of order zero,

$$\frac{\partial^2 p}{\partial r^2} + \frac{1}{r} \frac{\partial p}{\partial r} + k^2 p = Q(r), \quad (5)$$

where $k = \omega/c$ and $Q(r) = -(W/c^2)\exp(-r^2/2\sigma^2)$. To obtain a solution that is finite and unique we impose the boundary conditions $|p(0)| < \infty$ and

$$\lim_{r \to \infty} \sqrt{r} \left(\frac{dp}{dr} + ikp \right) = 0.$$

The second condition is known as the Sommerfeld radiation condition, which ensures that the pressure wave is moving outward [15].

Using the method of variation of parameters, we find that the general solution of (5) can be expressed in terms of the Hankel functions $H_0^{(1)}$ and $H_0^{(2)}$ [16] as

$$p(r) = \left[B_1 + c_1(r)\right]H_0^{(1)}(kr) + \left[B_2 + c_2(r)\right]H_0^{(2)}(kr), \quad (6)$$

where

$$c_1(r) = -\frac{\pi i}{4} \int_0^r s H_0^{(2)}(ks) Q(s) \, ds,$$
$$c_2(r) = \frac{\pi i}{4} \int_0^r s H_0^{(1)}(ks) Q(s) \, ds.$$

Making use of the boundary conditions, we find that $B_1 = B_2 = -\lim_{r \to \infty} c_1(r)$, and so the solution of (1) is

$$P(r,t) = p(r)\exp(i\omega t) = \left[f_1(r) - i f_2(r)\right]\exp(i\omega t), \quad (7)$$

where

$$f_1(r) = \frac{-\pi W}{2c^2} \left[\left(\int_r^\infty s Y_0(ks)\exp(-s^2/2\sigma^2) \, ds \right) J_0(kr) \right.$$
$$\left. + \left(\int_0^r s J_0(ks)\exp(-s^2/2\sigma^2) \, ds \right) Y_0(kr) \right], \quad (8)$$
$$f_2(r) = \frac{\pi W}{2c^2} \left(\int_0^\infty s J_0(ks)\exp(-s^2/2\sigma^2) \, ds \right) J_0(kr). \quad (9)$$

Here J_0 and Y_0 are the zeroth-order Bessel functions of the first and second kinds, respectively [16]. Then, taking the imaginary part of (7), the acoustic pressure wave is given by

$$P(r,t) = A(r)\sin(\omega t - \theta(r)), \quad (10)$$

where $A(r) = \sqrt{f_1(r)^2 + f_2(r)^2}$ and $\theta(r) = \arctan(f_2(r)/f_1(r))$ are the amplitude and phase, respectively.

To more readily identify how the pressure depends on radial distance, r, from the axis of the beam and on the width,

σ, of the beam we approximate the integrals (8) and (9) by using the change of variables $u = ks$ to obtain

$$f_1(r) = \frac{-\pi W}{2c^2 k^2} \big[g(r,k) J_0(kr) + h(r,k) Y_0(kr) \big],$$
$$f_2(r) = \frac{\pi W}{2c^2 k^2} h(\infty, k) J_0(kr), \tag{11}$$

where

$$g(r,k) = \int_{kr}^{\infty} u Y_0(u) \exp\!\big(-u^2/2(k\sigma)^2\big)\, \mathrm{d}u,$$
$$h(r,k) = \int_{0}^{kr} u J_0(u) \exp\!\big(-u^2/2(k\sigma)^2\big)\, \mathrm{d}u. \tag{12}$$

When $r \gg \sigma$,

$$f_1(r) - \mathrm{i} f_2(r) \approx \frac{-\pi W}{2c^2 k^2} h(\infty, k)\big[Y_0(kr) + \mathrm{i} J_0(kr) \big]. \tag{13}$$

Using the degree-one Taylor approximation $u J_0(u) \approx u$, we conclude that when $r \gg \sigma$, (10) is well approximated by

$$P(r,t) \approx A\left[J_0\!\left(\frac{\omega r}{c}\right) \cos(\omega t) + Y_0\!\left(\frac{\omega r}{c}\right) \sin(\omega t) \right], \tag{14}$$

where

$$A = (\gamma - 1)\omega \kappa_{\mathrm{eff}} W_{\mathrm{L}}/8c^2. \tag{15}$$

Equation (15) illustrates an important difference between the optically generated sound in unbounded space and in an enclosed volume (such as an acoustic resonator). It is well known that the amplitude of the photoacoustic wave in an enclosed cell scales as $1/\omega$ [9], whereas in (15) the amplitude scales proportional to ω. The physical reason for this difference is that in an enclosed cell the optical energy absorbed by the gas is accumulated in the cell, i.e. it is integrated over the duration of the modulation period. Therefore, the pressure amplitude is proportional to $1/\omega$. On the other hand, in unbounded space the energy is constantly carried away by the outgoing sound wave, and so the acoustic pressure is proportional to the speed of the optical power variation, and hence to ω. In experiments the width of the laser beam is narrow compared to the gap between the tines of the tuning fork. Therefore, as we will demonstrate in Sect. 3, we can use (14) to accurately compute the pressure wave in the vicinity of the tines. The approximation in (14) is the general form of an outgoing cylindrically symmetric pressure wave far from its source [14]. Equations (10) and (14) enable us to examine the range of validity of this approximation and to determine how the amplitude A depends on the parameters in the model. In particular, (14) shows that A is proportional to the modulation frequency ω, and is independent of the beam width σ when $r \gg \sigma$.
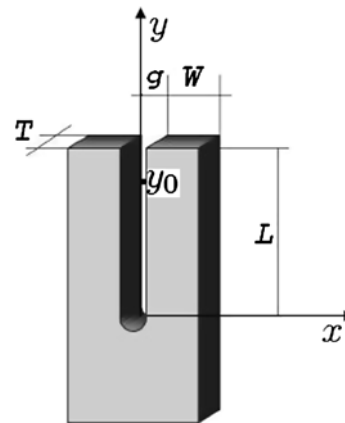
Fig. 1 The dimensions and coordinate system of the tuning fork. The origin of the x axis is centered between the tines and the origin of the y axis is at the junction of the tuning fork

2.2 Model for the vibration of the tuning fork

The acoustic pressure wave generated by the absorption of the optical energy causes the tines of the tuning fork to vibrate. In this section we present the second stage of the model, namely that which describes the motion of the tines. We regard the quartz tuning fork as a system of two weakly coupled beams, which we approximate as a pair of independent cantilevers each with a fixed end [10, 17]. As such, the tuning fork has two vibrational modes that correspond to in-plane motion of the tines, each with a different natural frequency. The electrodes of the quartz tuning fork are configured in such a way that only the symmetric mode (in which the tines move symmetrically with respect to the plane of symmetry of the tuning fork) induces an electrical signal. In the experimental system we center the acoustic source on the y as axis shown in Fig. 1 and we select the resonance frequency corresponding to the symmetric mode. When operated in this manner the QEPAS sensor is immune to background acoustic noise sources on either side of the tuning fork.

Let y denote the distance along the axis of a tine of the tuning fork from its base as shown in Fig. 1, and let $u(y,t)$ be the displacement at time t of a point at position y. Since the displacement is close to zero near the base of the tuning fork, we regard the two tines of the tuning fork as vibrating independently of each other. Furthermore, because the length of the tine, L, is considerably larger than its width, W, and thickness, T (see Fig. 1), we can regard each tine as a vibrating one-dimensional beam (cantilever). We assume that the beam is stationary at $y = 0$ and that the top of the beam is at $y = L$.

The damped motion of a vibrating beam is described by the Euler–Bernoulli equation [18]

$$\frac{EI}{\rho A} \frac{\partial^4 u}{\partial y^4} + 2\beta \frac{\mathrm{d}u}{\mathrm{d}t} + \frac{\partial^2 u}{\partial t^2} = \frac{1}{\rho A} f(y,t). \tag{16}$$

The parameters of a tine are Young's modulus, E, the second moment of area, I, the cross-sectional area, $A = TW$, the damping coefficient, 2β, and the density of quartz, ρ. Since the beam is fixed at $y = 0$ and free at $y = L$, we use the boundary conditions $u(0, t) = 0$, $(\partial u/\partial y)(0, t) = 0$, i.e. the displacement and slope at the fixed end are zero, and $(\partial^2 u/\partial y^2)(L, t) = 0$ and $(\partial^3 u/\partial y^3)(L, t) = 0$, i.e. the bending moment $EI(\partial^2 u/\partial y^2)$ and the shear force $(\partial/\partial y)(EI(\partial^2 u/\partial y^2))$ at the free end are zero [18].

The force density $f(y, t)$ on the right-hand tine is given by the difference between the acoustic pressure at the inner and outer surfaces of the tine multiplied by the thickness of the tine, namely

$$f(y, t) = T\left[P\left(\frac{g}{2}, y, t\right) - P\left(W + \frac{g}{2}, y, t\right)\right]. \tag{17}$$

Here T is the thickness of the tine, g is the gap between the tines of the tuning fork, and $P = P(x, y, t)$ is the acoustic pressure in the Cartesian coordinate system of the tuning fork. A formula for the pressure P in the polar coordinate system (r, θ) of the laser beam was derived in Sect. 2.1 and is given by (10). For simplicity we assume that the laser beam is symmetrically centered between the tines on the y axis at height $y = y_0$. Using the coordinate transformation $(x, y) = (r\cos\theta, y_0 + r\sin\theta)$ and the decomposition $P(r, t) = p(r)\exp(i\omega t)$ in (7), we find that the force density can be expressed in terms of the laser beam position, y_0, as

$$f(y, t; y_0) = f(y; y_0)\exp(i\omega t)$$
$$= T\left[p(r_i) - p(r_o)\right]\exp(i\omega t), \tag{18}$$

where

$$r_i = \left[\left(\frac{g}{2}\right)^2 + (y - y_0)^2\right]^{1/2},$$

$$r_o = \left[\left(W + \frac{g}{2}\right)^2 + (y - y_0)^2\right]^{1/2}.$$

Following [18, 19], the solution u of (16) is given by

$$u(y, t) = \sum_{n=1}^{\infty} B_n(y_0)\exp\left[i\left(\omega t - \delta_n(y_0)\right)\right]\Phi_n(y), \tag{19}$$

where $\Phi_n(y)$ is the nth eigenfunction of (16) with eigenfrequency ω_n, as given in [18]. Here

$$B_n(y_0) = \frac{|M_n(y_0)|}{\sqrt{(\omega_n^2 - \omega^2)^2 + 4(\beta\,\omega)^2}},$$

and

$$\tan\left(\delta_n(y_0)\right) = \frac{2\beta\omega\Re(M_n) - (\omega_n^2 - \omega^2)\Im(M_n)}{2\beta\omega\Im(M_n) + (\omega_n^2 - \omega^2)\Re(M_n)},$$

where $\Re$ and $\Im$ denote real and imaginary parts, and

$$M_n(y_0) = \frac{1}{\rho A}\frac{\int_0^L f(y; y_0)\Phi_n(y)\,dy}{\int_0^L \Phi_n^2(y)\,dy}. \tag{20}$$

We choose the forcing frequency, ω, to be equal to the frequency of the symmetric vibration of the tuning fork tines in the x direction. Since the tuning fork resonances are sharp, the displacement of each tine due to the acoustic pressure wave is given by

$$u(y, t) = \frac{|M_1(y_0)|}{2\beta\omega}\Phi_1(y)\sin\left(\omega t - \delta_1(y_0)\right), \tag{21}$$

where we have used the approximation $\omega_1 = \omega$.

2.3 Model of the piezoelectric response of the tuning fork

In the third stage of the model, we describe the relation between the amplitude of the oscillation of the end of a tine and the piezoelectric signal induced by the vibration of the two tines [11, 12].

The relationship between the charge $q(t)$ generated on one tine of the tuning fork and the deflection $u_L(t) = u(L, t)$ of its end point is given by $q = \alpha u_L$, where α is the effective piezoelectric coupling constant. Since we are assuming that the laser beam is centered on the plane of symmetry of the tuning fork, the maximum piezoelectric current, $\mathcal{I}$, generated by the two tines of the tuning fork is $\mathcal{I} = 2\alpha v$, where v is the maximum velocity of the end point of a tine. To determine α we first observe that by (21) the deflection u_L satisfies a damped spring–mass equation. As in [11] we choose the effective mass m_e of this spring–mass system so that the maximum total kinetic energy of the tine is $(1/2)m_e v^2$. Therefore, $m_e = m(1/L)\int_0^L \Phi_1^2(y)\,dy/\Phi_1^2(L) \simeq 0.25m$, where m is the physical mass of the tine. The effective spring constant is defined by $k_e = m_e\omega^2$, where ω is the resonance frequency of the tine. When making measurements we regard the tuning fork as an RLC circuit with electrical parameters $\mathcal{R}$, $\mathcal{L}$, and $\mathcal{C}$ [12]. Since energy is conserved, the piezoelectric current, $\mathcal{I}$, is also related to the common speed v of the end points by $2(m_e v^2/2) = \mathcal{L}\mathcal{I}^2/2$. Therefore, $\mathcal{L} = m_e/2\alpha^2$ and, since $\omega^2 = k_e/m_e = 1/\mathcal{L}\mathcal{C}$, we have $\mathcal{C} = 2\alpha^2/k_e$. Since the quality factor can be expressed in terms of both the mechanical and electrical parameters as $Q = \omega/2\beta = \sqrt{\mathcal{L}/\mathcal{C}}/\mathcal{R}$, we conclude that $\alpha = \sqrt{m_e\omega/2Q\mathcal{R}}$, which can be obtained from measured values of the quality factor Q and resistance $\mathcal{R}$. Finally, by (21), when the laser is centered at $y = y_0$ on the y axis the maximum piezoelectric current is

$$\mathcal{I}(y_0) = \frac{\alpha\Phi_1(L)}{\beta}|M_1(y_0)|. \tag{22}$$

3 Results

3.1 Experimental setup

We performed two sets of experiments to validate the model. For the first set we used a standard QTF with a resonance frequency of 32.8 kHz and for the second set we compared the standard QTF to a large QTF with a resonance frequency of 4.25 kHz. The dimensions and parameters of the tuning forks are listed in Table 1. Young's modulus and the density of quartz are $E = 78.7$ GPa and $\rho = 2.6 \times 10^3$ kg/m^3, respectively [17].

In both sets of experiments, a laser beam was directed between the tines of the tuning fork at a vertical position y_0 on the symmetry axis of the fork (see Fig. 1). The beam waist radius was estimated to be $\sigma = 0.05$ mm. The diode laser injection current was modulated at half the resonance frequency of the tuning fork, as is done in most QEPAS detection schemes utilizing $2f$ wavelength modulation spectroscopy.

For the first set of experiments, the QTF was enclosed in a cylindrical optical gas cell and measurements were performed using a 1000 ppmv NH$_3$:N$_2$ gas mixture. The optical frequency of the diode laser was centered on the 6528.80 cm^{-1} NH$_3$ absorption line. The speed of sound in N$_2$ at room temperature is $c = 346$ m/s and the adiabatic coefficient of N$_2$ is $\gamma = 1.4$. The experiments were performed at total gas pressures of 450 Torr and 60 Torr. The measured QTF parameters for these two pressures and the derived effective piezoelectric coupling constant, α, are shown in Table 2, together with the value of κ_{eff} calculated using (2). The calculation of the effective absorption coefficient was based on spectroscopic data from Webber et al. [20]. Simulated absorption spectra based on these parameters show some discrepancy with experimental observations; in particular, pressure-induced shifts appear to be present. We compared the signal produced by our NH$_3$ mixture with the signal generated by 10 ppmv C$_2$H$_2$:N$_2$ gas when a well-characterized 6523.87 cm^{-1} line (P(13) of the $\nu_1 + \nu_3$ band) is excited. In both cases, the optimum wavelength-modulation width, λ_{amp}, and the corresponding maximum value of κ_{eff} were calculated for a total pressure of 450 Torr based on the available data (Webber et al. [20] for NH$_3$ and the HITRAN 2004 database for C$_2$H$_2$). Then, the actual experimental measurements were performed and the measured QEPAS signals compared. The agreement between the ratio of the calculated κ_{eff} and the observed signals is within 20%.

Since the large QTF did not fit into the available optical gas cell, the second set of experiments was performed in the open, using the ambient moisture (typically 50% relative humidity at +24°C) and a diode laser centered on the 7306.75 cm^{-1} H$_2$O absorption line.

Table 1 Dimensions and parameters of the standard and large tuning forks: f (frequency), L (length), T (thickness), W (width), g (gap), and I (second moment of area)

| Parameter	SI unit	Standard	Large
f	kHz	32.8	4.25
L	mm	3.8	20
T	mm	0.34	0.79
W	mm	0.6	1.95
g	mm	0.3	1.24
$I = \frac{TW^3}{12}$	m^4	6.12×10^{-15}	4.88×10^{-13}

Table 2 Measured physical parameters for experiments performed using a 32.8 kHz tuning fork: f (modulation frequency), Q (quality factor), $\mathcal{R}$ (resistance), α (effective piezoelectric coupling constant), W_L (laser power), and κ_{eff} (effective absorption coefficient).

Parameter	SI unit	450 Torr	60 Torr
f	kHz	32.761	32.764
Q	–	16 064	28 887
$\mathcal{R}$	kΩ	111	62
α	C/m	7×10^{-6}	7×10^{-6}
W_L	mW	61.7	62.1
κ_{eff}	cm^{-1}	1.31×10^{-4}	9.57×10^{-4}

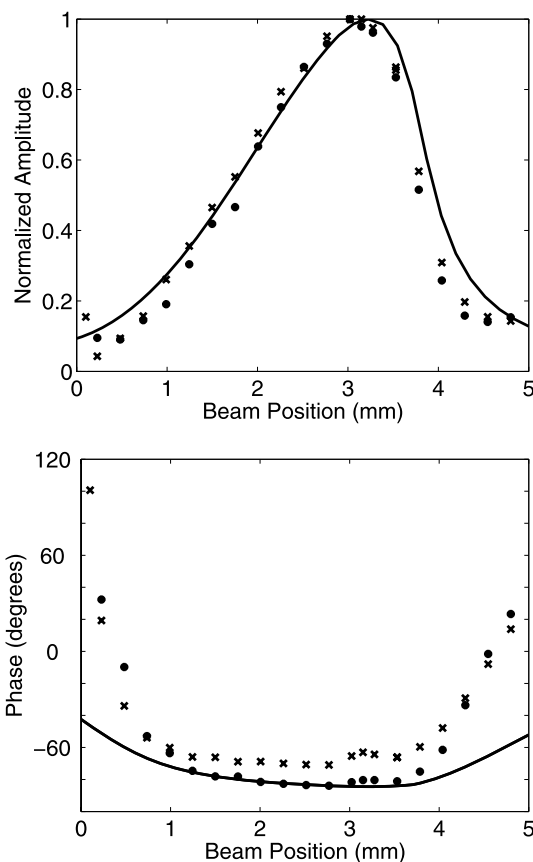## 3.2 Theoretical and experimental results

We begin by comparing the acoustic pressure waves generated using the two modulation frequencies. In the top half of Fig. 2 we plot the amplitude and in the bottom half we plot the phase of the acoustic pressure wave as a function of the radial distance, r, from the center of the laser beam. The solid and dashed curves show the results for the 32.8 kHz and 4.25 kHz modulation frequencies, respectively, obtained from (8)–(10) using numerical integration. For both modulation frequencies we used the measured values of the laser power, W_L, and effective absorption coefficient, κ_{eff}, at 450 Torr given in Table 2. We observe that the amplitude of the acoustic pressure is larger for the 32.8 kHz than for the 4.25 kHz modulation frequency. The dotted curves show the approximation (14) of the exact solution (10) for the 32.8 kHz modulation frequency. This result shows that the approximation (14) is valid for $r > 0.1$ mm. Since the gap g between the tines satisfies $g/2 \geq 0.15$ mm, we can use (14) to calculate the pressure wave in the vicinity of the tines of the tuning fork. These results are used in the second stage of the model to calculate the vibration of the tines of the tuning fork.

In previous experimental work, Kosterev et al. [4] found that the response of the 32.8 kHz tuning fork was largest when the laser beam was centered between the tines and positioned 0.7 mm below the opening of the tuning fork
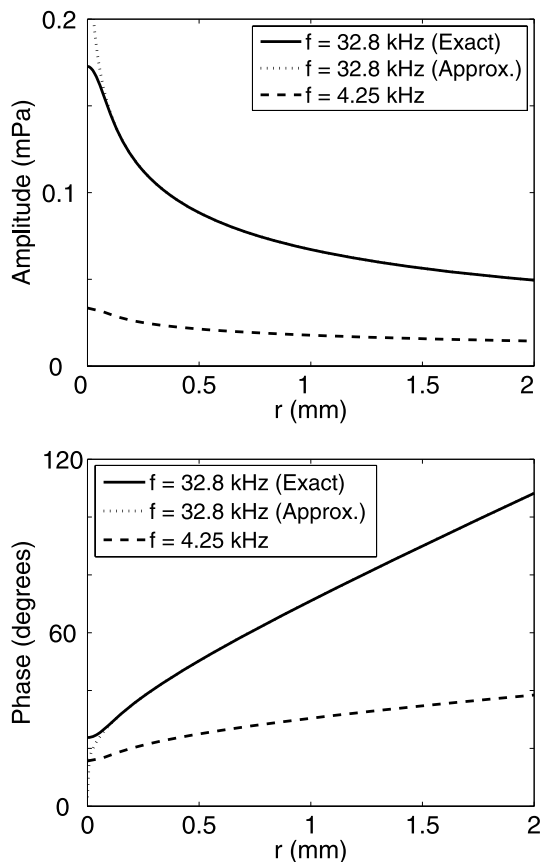
Fig. 2 The amplitude (*top*) and phase (*bottom*) of the acoustic pressure wave as a function of the radial distance r from the center of the laser beam. The *solid* and *dashed curves* shows the results for the 32.8 kHz and 4.25 kHz modulation frequencies, respectively, as computed using the exact formulae (8)–(10). The *dotted curves* show the result for the 32.8 kHz modulation frequency computed using the approximation (14) of (10). The *solid* and *dotted curves* overlap for $r > 0.1$ mm

Fig. 3 Normalized amplitude (*top*) and phase (*bottom*) of the piezo-electric current as functions of the vertical position, y_0, of the laser beam for a QEPAS sensor with a 32.8 kHz tuning fork. The theoretical results are shown with *solid lines*, and the experimental data measured at 450 Torr and 60 Torr are shown with *dots* and *crosses*, respectively. These results are from the first set of experiments using the NH_3:N_2 mixture

($y_0 = 3.1$ mm). In the top half of Fig. 3 we show the normalized amplitude and in the bottom half we show the phase of the piezoelectric current as functions of the laser beam position, y_0. The experimental results were obtained from the first set of experiments using the NH_3:N_2 mixture. We show the theoretical results computed using (22) with solid lines, the experimental data measured at 450 Torr with dots, and the experimental data measured at 60 Torr with crosses. We separately normalized the three amplitude curves in the top half of Fig. 3 to have maximum values of 1. The theoretical normalized amplitude and phase are independent of the ambient pressure. The theoretical and experimental normalized amplitudes agree extremely well. In particular, the theory confirms the experimentally observed optimal position of the laser beam. In the bottom half of Fig. 3 we show that the theoretically computed phase of the current is in excellent agreement with the experimental data at 450 Torr over the interval $1.25 < y_0 < 3.75$.

The phase lag at 60 Torr is explained by the vibrational to translational (V–T) energy-transfer delay from the optically excited state of NH_3. In the case of a single-step population decay with time constant, τ, the phase lag, θ, due to V–T relaxation is given by $\tan \theta = \omega \tau$ [21]. From the experimental data, $\theta = 15°$, as measured near $y_0 = 3.2$ mm. The τ value derived from a 15° phase lag is 1.24 μs. Therefore, the V–T relaxation time constant is $\tau P = 98$ ns atm, and the corresponding rate constant is $k_{V–T} = 4.3 \times 10^{-13}$ cm^3/molecule s^{-1}. We did not find the V–T relaxation rate from this state reported in the literature. However, in [22] the relaxation rate from the ν_2 excited state of NH_3 in N_2 was measured as $k_{V–T} = 3.6 \times 10^{-13}$ cm^3/molecule s^{-1}. Therefore, our results are realistic.

In Table 3, we show the maximum amplitude of the piezoelectric current for the 32.8 kHz tuning fork. In absolute units the theoretically calculated amplitudes are about two times smaller than the measured values. We do not know whether this discrepancy is due to a missing factor of two in

Table 3 The theoretical and experimental maximum amplitudes of the piezoelectric current

Pressure (Torr)	Theory (pA)	Experiment (pA)
60	45.2	81.6
450	35.0	72.3

the theory, errors in the parameter values, or physical limitations of the model.

For the second set of experiments we did not make absolute measurements of the signal strength. Rather, the experiments for the 4.25 kHz and 32.8 kHz tuning forks were performed under identical conditions and the ratio of the signal strengths was calculated. Consequently, in this case we did not need to measure the effective absorption coefficient of the gas. The effective piezoelectric coupling constant of the 4.25 kHz tuning fork was found to be $\alpha = 8.88 \times 10^{-6}$ C/m. The theoretical normalized amplitude and the phase of the current are very similar to the results we obtained for the 32.8 kHz tuning fork except that the optimal beam position is at $y_0 = 17.5$ mm (2.5 mm below the opening). In these experiments, the maximum amplitude was 2.2 times larger for the 32.8 kHz than for the 4.25 kHz tuning fork, while the theoretically computed ratio was 2.9. We conclude that, in a QEPAS sensor with this simple configuration, it is preferable to use the 32.8 kHz rather than the 4.25 kHz QTF we had available, since the 32.8 kHz QTF not only produces a stronger signal but is more compact in size and is less susceptible to environmental acoustic noise.

4 Conclusions

We developed a theoretical model for a QEPAS sensor that enables the piezoelectric signal to be expressed in terms of the optical, mechanical, and electrical parameters of the system. To derive an analytical solution for this model we used several physically reasonable assumptions to simplify the geometry of the problem and reduce the governing partial differential equations to ordinary differential equations. In particular, we ignored the effect the tuning fork has on the acoustic pressure wave, and we assumed that the piezoelectric response of the tuning fork can be obtained by modeling each tine individually. In spite of these simplifying assumptions, we obtain excellent agreement between theory and experiments. The model accurately predicts the optimal location of the laser beam relative to the tuning fork, the phase of the piezoelectric current relative to that of the optical radiation, and the dependence of the signal strength on the laser modulation frequency.

In future work, we will extend the model to describe a QEPAS sensor in which a weak resonator consisting of a

pair of cylindrical tubes is added on either side of the tuning fork to enhance the sensitivity of the sensor. This extension will require us to numerically solve the acoustic wave equation in three spatial dimensions with appropriate boundary conditions. The resulting acoustic pressure field will then be input into the tuning fork model described in this paper. This approach will also enable us to study any effects that the tuning fork has on the acoustic wave. Future extensions to the model described in this paper will enable us to further optimize QEPAS sensor design. Nonetheless, this paper provides the basis for future models.

References

1. A.A. Kosterev, G. Wysocki, Y. Bakhirkin, S. So, R. Lewicki, M. Fraser, F.K. Tittel, R.F. Curl, Appl. Phys. B **90**(2), 165 (2007)
2. M.R. McCurdy, Y. Bakhirkin, G. Wysocki, R. Lewicki, F.K. Tittel, J. Breath Res. **1**, 014001–014013 (2007)
3. T.H. Risby, S.F. Solga, Appl. Phys. B **85**(2–3), 421 (2006)
4. A.A. Kosterev, Y.A. Bakhirkin, R.F. Curl, F.K. Tittel, Opt. Lett. **27**(21), 1902 (2002)
5. A.A. Kosterev, F.K. Tittel, D.V. Serebryakov, A.L. Malinovsky, I.V. Morozov, Rev. Sci. Instrum. **76**(4), 0431051 (2005)
6. R. Lewicki, G. Wysocki, A.A. Kosterev, F.K. Tittel, Appl. Phys. B **87**(1), 157 (2007)
7. S.H. Yönak, D.R. Dowling, J. Acoust. Soc. Am. **114**(6), 3167 (2003)
8. A. Miklos, Z. Bozoki, Y. Jiang, M. Feher, Appl. Phys. B **58**, 483 (1994)
9. A. Miklos, P. Hess, Z. Bozoki, Rev. Sci. Instrum. **72**(4), 1937 (2001)
10. K. Karraï, R.D. Grober, Ultramicroscopy **61**(1), 197 (1995)
11. K. Karraï, R.D. Grober, Appl. Phys. Lett. **66**(14), 1842 (1995)
12. R.D. Grober, J. Acimovic, J. Schuck, D. Hessman, P.J. Kindlemann, J. Hespanha, S.A. Morse, K. Karraï, I. Tiemann, S. Manus, Rev. Sci. Instrum. **71**(7), 2776 (2000)
13. M.D. Wojcik, M.C. Phillips, B.D. Cannon, M.S. Taubman, Appl. Phys. B **11**(2–3), 307 (2006)
14. P.M. Morse, K.U. Ingard, *Theoretical Acoustics* (Princeton University Press, Princeton, 1986)
15. M.A. Pinsky, *Partial Differential Equations and Boundary Value Problems with Applications* (McGraw-Hill, New York, 1991)
16. A. Abramowitz, I.A. Stegun, *Handbook of Mathematical Functions* (Dover, New York, 1974)
17. D.V. Serebryakov, A.P. Cherkun, B.A. Loginov, V.S. Letokhov, Rev. Sci. Instrum. **73**(4), 1795 (2002)
18. C.R. Wylie, *Advanced Engineering Mathematics* (McGraw-Hill, New York, 1966)
19. A.P. French, *Vibrations and Waves* (Norton, New York, 1971)
20. M.E. Webber, D.S. Baer, R.K. Hanson, Appl. Opt. **40**(12), 2031 (2001)
21. G. Gorelik, Dokl. Akad. Nauk SSSR **54**, 779 (1946) (in Russian)
22. F.E. Hovis, C.B. Moore, J. Chem. Phys. **69**, 4947 (1978)